Terahertz Quantum Cascade Lasers based on two-dimensional photonic crystal resonators

Lorenzo Sirigu, Romain Terazzi, Maria. I. Amanti, Marcella Giovannini and Jérôme Faist

Institute of Physics, University of Neuchâtel, CH-2000 Neuchâtel, Switzerland

lorenzo.sirigu@unine.ch

L. Andrea Dunbar and Romuald Houdré

Institute of Photonics and Quantum Electronics, Swiss Federal Institute of Technology Lausanne-EPFL, CH-1015, Lausanne, Switzerland

Abstract: We demonstrate high spectral control from surface emitting THz Quantum Cascade Lasers based on a two-dimensional photonic crystal cavity. The perforated top metallic contact acts as an in plane resonator in a tight double-metal plasmonic waveguide providing a strong optical feedback without needing three-dimensional cavity features. The optical far-field patterns do not exhibit the expected symmetry and the shape of the cavity mode. The difference is attributed to a metal surface plasmon mediated light outcoupling mechanism also responsible for the relatively low extraction efficiency.

OCIS codes: (140.5965) Semiconductor lasers, quantum cascade; (140.3070) Infrared and far-infrared lasers; (130.5296) Photonic crystal waveguides; (240.6680) Surface plasmons

References and links

1. J. Faist, F. Capasso, D. L. Sivco, C. Sirtori, A. L. Hutchinson, and A. Y. Cho, "Quantum Cascade Laser," Science **264,** 553–556 (1994).
2. R. Köhler, A. Tredicucci, F. Beltram, H. E. Beere, E. H. Linfield, A. G. Davies, D. A. Richie, R. C. Lotti, and F. Rossi "Terahertz semiconductor-heterostructure laser," Nature **417,** 156–159 (2002).
3. L. Mahler, R. Köhler, A. Tredicucci, F. Beltram, H. E. Beere, E. H. Linfield, D. A. Ritchie, and A. G. Davies "Single-mode operation of terahertz quantum cascade lasers with distributed feedback resonators," Appl. Phys. Lett. **84,** 5446–5448 (2004).
4. J. A. Fan, M. A. Belkin, F. capasso, S. Khanna, M. Lachab, A. G. Davies, and E. H. Linfield "Surface emitting terahertz quantum cascade laser with a double-metal waveguide," Opt. Express **14,** 11672-11680 (2006). http://www.opticsinfobase.org/abstract.cfm?URI=oe-14-24-11672
5. S. Kumar, B. S. Williams, Q. Quin, A. W. Lee, Q. Hu, and J. L. Reno "Surface-emitting distributed feedback terahertz quantum-cascade lasers in metal-metal waveguides," Opt. Express **15,** 113-128 (2007). http://www.opticsinfobase.org/abstract.cfm?URI=oe-15-1-113
6. G. Fashing, A. Benz, K. Unterrainer, R. Zobl, A. M. Andrews, T. Roch, W. Schrenk, and G. Strasser "Terahertz microcavity quantum cascade lasers," Appl. Phys. Lett., **87,** 211112 (2005).
7. Y. Chassagneux, J. Palomo, R. Colombelli, S. Dhillon, C. Sirtori, H. Beere, J. Alton, and D. Ritchie, "Terahertz microcavity lasers with subwavelength mode volumes and thresholds in the milliampere range," Appl. Phys. Lett., **90,** 091113 (2006)
8. B. S. Song, S. Noda, T, Asano and Y. Akahane, "Ultra-high-Q photonic double-heterostructure nanocavity," Nature Materials **4,** 207-210 (2005).
9. H. G. Park, S. H. Kim, S. H. Kwon, Y. G. Ju, J. K. Yang, J. H. Baek, S. B. Kim, and Y. H. Lee, "Electrically Driven Single-Cell Photonic Crystral Laser," Science **305**, 1444-1447 (2004).

#91091 - $15.00 USD Received 21 Dec 2007; revised 29 Feb 2008; accepted 20 Mar 2008; published 1 Apr 2008

10. I, Vurgaftman and J. R. Meyer, "Photonic-Crystal Distributed-Feedback Quantum Cascade Lasers" IEEE J. Quantum Electron., **38,** 592-602 (2002).
11. M. Kim, C. S. Kim, W. W. Bewley, J. R. Lindle, C. L. Canedy, I. Vurgaftman, and J. R. Meyer, "Surface-emitting photonic crystal distributed-feedback laser for the midinfrared," Appl. Phys. Lett. **88,** 191105 (2006).
12. L. A. Dunbar, V. Moreau, R. Ferrini, R. Houdré, L. Sirigu, G. Scalari, M. Giovannini, N. Hoyler and J. Faist, "Design, Fabrication and Optical Characterisation of Quantum Cascade Lasers at Terahertz Frequencies using Photonic Crystal Reflectors," Opt. Express **13,** 8960-8968 (2005). http://www.opticsinfobase.org/abstract.cfm?URI=oe-13-22-8960
13. A. Benz, G. Fasching, C. Deutsch, A. M. Andrews, K. Unterrainer, P. Klang, W. Schrenk, and G. Strasser "Terahertz photonic crystal resonators in double-metal waveguides," Opt. Express **15,** 12418-12424 (2007). http://www.opticsinfobase.org/abstract.cfm?URI=oe-15-19-12418
14. H. Zhang, L. A. Dunbar, G. Scalari, R. Houdré, and J. Faist "Terahertz photonic crystal quantum cascade lasers," Opt. Express **15,** 16818-16827 (2007) http://www.opticsinfobase.org/abstract.cfm?URI=oe-15-25-16818
15. R. Colombelli, K. Srinivasan, M. Troccoli, O. Painter, C. F. Gmachl, D. M. Tennant, A. M. Sergent, D. L. Sivco, A. Y. Cho, and F. Capasso "Quantum Cascade Surface-Emitting Photonic Crystal Laser," Science **302,** 1374–1377 (2003).
16. G. Scalari, L. Sirigu, R. Terazzi, C. Walther, M. I. Amanti, M. Giovannini, N. Hoyler, J. Faist, M. L. Sadowski, H. Beere, D. Ritchie, L. A. Dunbar, R. Houdré "Multi-wavelength operation and vertical emission in THz quantum-cascade lasers" J. Appl. Phys. **101,** 081726 (2007).
17. S. Johnson and J. Joannopoulos "Block-iterative frequency-domain methods for Maxwell's equations in a planewave basis," Opt. Express **8,**, 173-190 (2001).
18. G. Scalari, N. Hoyler, M. Giovannini, and J. Faist "Terahertz bound-to-continuum quantum-cascade lasers based on optical-phonon scattering extraction," Appl. Phys. Lett. **86,** 181101-3 (2005).
19. K. Srinivasan, P. E. Barclay, M. Borselli, and O. Painter "Optical-fiber-based measurements of ultrasmall volume high-Q photonic crystal microcavity," Phys. Rev. B **70,** 081306 (2004).

1. Introduction

Quantum cascade lasers (QCLs) have been established in the last 10 years as one of the light source of choice in the mid-infrared portion of the electromagnetic spectrum[1]. Since the first demonstration of QCLs emitting below the restrahlen band region[2], new opportunities were opened for using these devices in a large variety of applications such as terahertz (THz) imaging for biological and biomedical research, astronomy, and scanning imaging for homeland security.

Most THz QCLs fabricated so far, were relying on a standard Fabry Perot cavity design combined with a ridge geometry for confining light in the direction perpendicular to the light propagation axis. Patterning of the top contact metal layer has been successfully introduced more recently in THz QCLs in order to obtain a frequency selected laser emission both in single-plasmon[3] and double metal waveguide configuration[4, 5]. The main advantage of this approach is the straightforward fabrication process, but the main drawbacks are the strong beam divergence and ellipticity, and the higher waveguide losses with respect to the single plasmon waveguide configuration. Alternative cavity designs, like microcavity or microring resonators, address the size issue, but don't provide a fine spectral control of the lasing emission [6, 7].

Two-dimensional photonic crystal (PhC) structures are the natural candidate to provide an elegant solution for the spectral control and to try to control the mode pattern and beam shape. Very tight optical confinement with ultra-high cavity quality factors [8], and miniaturization of the optical resonator in laser emitters [9], has been recently proved for PhC -based devices and are induced by the intrinsic flexibility of the PhC approach. The first attempts aimed to integrate PhC patterning in mid -IR lasers, were oriented towards a two-dimensional evolution of the standard DFB lasers by replacing a standard grating with a tilted 2D PhC in order to enhance the spectral purity [10]. Vertical emission from an optically pumped mid-infrared laser was also demonstrated from J. R. Meyer and coworkers in PhC DFB laser [11]. At terahertz frequencies, 2D PhC Bragg mirrors were used with QCLs in a single-plasmon waveguide configuration to obtain single mode lasing emission from a standard ridge laser[12]. A similar approach involving an active core surrounded by a PhC resonator embedded in a double metal waveguide

#91091 - $15.00 USD Received 21 Dec 2007; revised 29 Feb 2008; accepted 20 Mar 2008; published 1 Apr 2008

was proposed by Benz and coworkers [13]. In this work the PhC structures acts as a spectral filter applied to a conventional THz QCL active structure.

Finally, recent developments led to in-plane lasing from an array of THz QCL pillars[14]. The pillars were arranged in such a way that the ensemble was at the same time the optical resonator and the laser active region. Similarly to [12], the laser operated on PhC band edge configuration and reached very low threshold currents and high spectral control.

However, the first attempt to achieve vertical emission using PhC as optical resonator in a plasmonic waveguide integrated directly into the active region of the laser device, came from Colombelli and coworkers in 2003[15] in the mid-infrared region. The combination of a PhC-based microresonator with the vertical emission, address in this case both the device size and the spectral selectivity issues.

The same approach was successively extended to the THz region[16] but with poor performance due to the high optical losses induced by the high filling factor of the PhC structure in the double metal waveguide configuration. Moreover, in this early work the relative small lateral dimensions of the devices translated in a strong dependence of the emission pattern from the device metallic edge.

In the work presented in this article, we have designed and fabricated a THz QCL based on an in-plane resonator that relies on a 2D metallic PhC that allows lasing emission along the vertical direction. The PhC is realized by removing only the metal and the doped contact layer from the corresponding lattice sites of the top surface. This configuration, which achieves a relatively low index contrast, proved to give a very good spectral control of the laser emission with single mode behavior for most of the tested devices. Moreover, a spectral tuning is obtained by varying the PhC parameters. Photonic band dispersion calculated with the plane wave expansion method [17] lead to a clear attribution of the laser modes.

An analysis of the far-field patterns recovered from the top surface of the devices is also presented, showing that the surface plasmon excited in the top metallic layer dominates in the light extraction, and this translates in a low optical power and in a broad angular dispersion of the optical mode. An improved light extraction efficiency is observed in preliminary results compared with samples with deep etched PhC cavites.

2. Design and fabrication

The active region of our THz QCL has been grown by Molecular Beam Epitaxy using the GaAs/AlGaAs material system. The active layer design is based on the bound-to-continuum concept combined with an optical phonon assisted extraction mechanism, similar to what described in ref.[18]. Such a design presents an intrinsic gain curve shift as a function of the applied bias which is reflected, in QCLs processed in a standard ridge waveguide configuration, in a bias voltage dependent spectral tuning. In order to provide both a tight vertical optical confinement and an increased optical coupling with the 2D PhC, the sample is processed in the double metal waveguide configuration. The processing consists in bonding the sample on a previously metallized n-doped GaAs substrate by means of Au/Au thermocompression wafer bonding. The original substrate was then selectively removed by a combination of mechanical polishing and selective wet etching. After defining the injection regions on the top surface with hexagonal openings in a passivating silicon nitride layer, the top surface was metallized with a thin (3/100 nm) Ti/Au layer. The PhC resonator is thus defined by the patterning of the metallic layer performed by standard lift-off techniques. The process was completed by the removal of the top heavily doped GaAs layer in the metal holes with a H_3PO_4:H_2O_2:H_2O (1:3:80) solution. For this first generation of devices, no mesa structures were etched to define the single hexagonal laser device, in order to avoid the presence of additional optical cavity modes that would have interfered with the PhC modes, scrambling the data interpretation. The draw back of this

#91091 - $15.00 USD Received 21 Dec 2007; revised 29 Feb 2008; accepted 20 Mar 2008; published 1 Apr 2008

choice is a current spreading below the silicon nitride layer that is difficult to quantify due to the uncertainty on the remaining thickness of the doped contact layer. A special care was used to keep very narrow opening (10 μm) between the rectangular contact pads, with the aim of preventing light leaks from the pad edges. The triangular lattice pattern that constitutes our PhC,

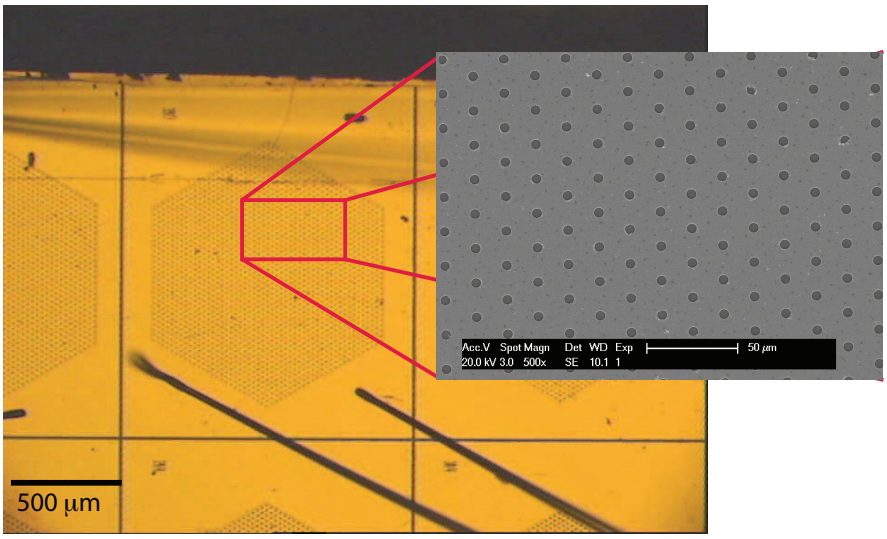

Fig. 1. Optical microscope image of a 2D PhC-based THz QCL. In the zoom area a scanning electron microscope detail of the PhC openings is shown.

was chosen because of its connected nature that guarantees a simple processing procedure, and a uniform current injection. This PhC geometry, does not generate a complete photonic band gap for TM-polarized light (electric field along the vertical axis)but still it presents low loss states both on slow light points at the edge of the band dispersion and in local minima in high symmetry points below the light cone [19]. The basic idea is that the PhC enables to select a series of modes of the surrounding cavity that are compatible with the energy dispersion relations of a crystal photon.

From a laser device perspective, only the very few modes that both match the energy dispersion of the PhC and the gain bandwidth of the active region, have losses low enough to allow laser action.

The band diagram drawn in Fig.2(a) represents the TM photon energy dispersion along the boundary of the first irreducible Brillouin zone (ΓMKΓ path) of a dielectric triangular lattice of holes. The modal index of a large double metal ridge waveguide ($\approx$ 3.71) is used for the bulk material, while the index in the holes is approximated to 2.2, corresponding roughly to the modal index of a ridge waveguide with the top metal removed. The ratio of the hole radius (r) over the lattice constant (a) in this simulation was kept at r/a = 0.14 (filling factor f = 7%). The relatively low effective index found for this simulation is due to the deep penetration of the optical mode in the air region. This situation is well presented in the 2D cross-sectional simulation shown in Fig.2(b) where an effective index n_{eff} = 2.21 is found. The simulation was carried out for a half-ridge structure composed, starting from the bottom, with a metallic layer, an active region with n_{eff} = 3.7, and air for the TM-polarized fundamental mode.

An array of devices with different r/a values were fabricated with "a" ranging between 18-22 μm and "r" ranging from 2 to 4 μm, in such a way to explore a wide region of the band dispersion. The relatively low values of the PhC filling factors, were chosen in order to minimize the waveguide losses otherwise prohibitive for a laser device at terahetz frequencies. This first

#91091 - $15.00 USD Received 21 Dec 2007; revised 29 Feb 2008; accepted 20 Mar 2008; published 1 Apr 2008

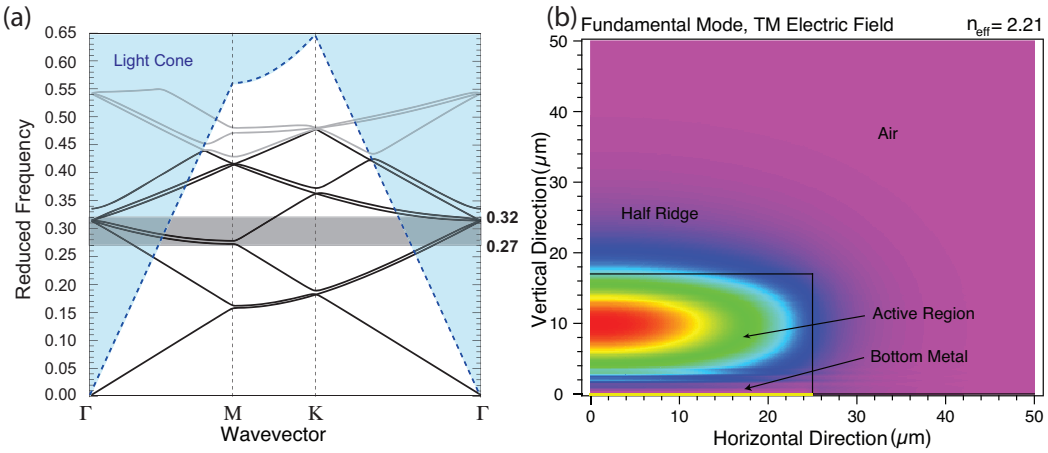

Fig. 2. (a) TM photon band diagram of a triangular lattice of holes along the ΓMKΓ path up to the 10^{th} band. The shaded blue region represents the light cone in air, whereas the horizontal gray band shows the energy range covered by the laser emission of our samples. (b) Two-dimensional simulation from a half-ridge structure composed by a bottom metallic layer, an active region with n_{eff} = 3.7, and air for the TM-polarized mode. The simulation was performed in order to assign the effective index of the mode taking into account the hole part of the device. An effective index n_{eff} = 2.21 was found.

family of devices was designed with a large number of PhC periods (25 per side) that allows sufficient feedback to achieve laser action.

Before measurements, array of samples were cleaved, soldered on a copper plate, and bonded. The measurements were performed on an He-flow cryostat integrated in a vacuum FTIR spectrometer where the emitted light was detected by a liquid He cooled bolometer. The samples were operated in pulsed regime with a duty cycle of $5{\cdot}10^{-5}$.

3. Measurements

The optical feedback provided by the 2D PhC proved to be strong enough for certain lattice parameters to allow lasing emission from the top surface. This is shown in Fig.3 where we plot the peak power vs injected current (LIV curves) taken at different temperatures from a device with r/a = 0.143. The laser was operated in pulsed regime with a duty cycle of $5{\cdot}10^{-5}$. The measured threshold current is $J_{th} \simeq 580$ A/cm^2 at T = 7 K and it reaches a maximum operating temperature of 95 K.

Nevertheless, these devices display a poor output power if compared to what is obtained in analogous ridge waveguide lasers fabricated with the same active region both in single-plasmon and double metal waveguide configuration. If the relatively small filling factor of the PhC structure may have a role in these limitations, it cannot be considered the main limiting factor. We will see later in this paper that the planar geometry of the PhC resonator combined with the excitation of a surface plasmon mode in the top metallic contact of the lasers, prevents from extracting the laser light with a low divergence and highly directional beam. Moreover, we will see that a partial breaking of this planar symmetry can considerably increase the extracted power changing significantly the optical mode pattern.

A series of lasing spectra taken from devices with different lattice constants ranging from 18 up to 22 μm is shown in Fig.4. All the devices are biased at comparable applied voltages ($\simeq$ 14 V) in order to discriminate from spectral shift eventually arising from Stark shift. All

#91091 - $15.00 USD Received 21 Dec 2007; revised 29 Feb 2008; accepted 20 Mar 2008; published 1 Apr 2008

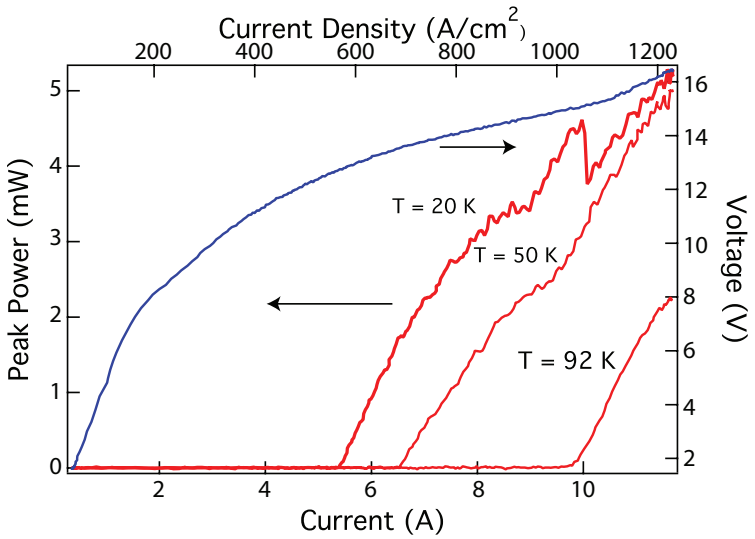

Fig. 3. Output optical peak power vs injected current curves taken at different temperatures. Lasing action was observed up to 95 K. The relatively high operating voltages are probably due to a double Schottky interface formed by the double metal waveguide metallic layer sequence.

the lasers, with the only exception of one with a = 19 μm, show single mode operation that is kept up to the LI roll-over for all devices with lattice constant a$\leq$ 20 μm. The absence of an additional external cavity and the selectivity on the laser frequency, prove that the PhC optical feedback is responsible for lasing. Moreover, different device dices were cleaved in order to assess the influence of the cleaved facets on the laser properties and no variations in threshold current nor in spectral emission were observed ruling out the role of the facets as cavity mirrors. Another striking feature of these laser devices is the large spectral window over which the lasing emission is tuned. This is in part due to the broad gain curve specific to the active region employed, as shown in Fig.4(b) where a subthreshold luminescence curve obtained from a ridge QCL processed in single-plasmon waveguide configuration is shown. Moreover, the PhC resonator push the active layer to lase up to the high energy tail of the gain curve, beyond what is usually observed in the standard Fabry Perot geometry. In order to assess the entity of the tuning range and separate it from a bias-induced stark blue-shift, it is worth noting that the estimated spectral blue shift of the luminescence emission from a standard ridge QCL based on the same active region is of $\approx$ 1 meV/V.

In order to establish the the physical origin of the lasing emission we refer to the plane wave expansion band dispersion diagram shown in Fig.2 that, we remind, has been calculated for r = 3 μm and a = 22μm. By comparing the band diagram with the energy positions of the main lasing peaks, we can attribute these latters to an optical feedback occurring on the M-point of the third and fourth PhC band. This region is situated at an energy that well overlap the central part of the gain curve and at the same time is situated below the light cone obtaining therefore a strong optical confinement for the generated light. This point is well illustrated in Fig.5(a), where we plot the same spectral evolution of Fig.4(a) in reduced energy units. From this figure one main peak at a/λ = 0.27 is observed for all the lasing devices, which perfectly overlap with the M-point position. The small spectral shift observed for lattice parameters a going from 19 μm to 20 μm is maybe caused by the transition from the 3^{rd} to the 4^{th} excited band across the bandgap on the M-point. This single mode behavior holds for all the samples with a$\leq$ 20 μm

#91091 - $15.00 USD Received 21 Dec 2007; revised 29 Feb 2008; accepted 20 Mar 2008; published 1 Apr 2008

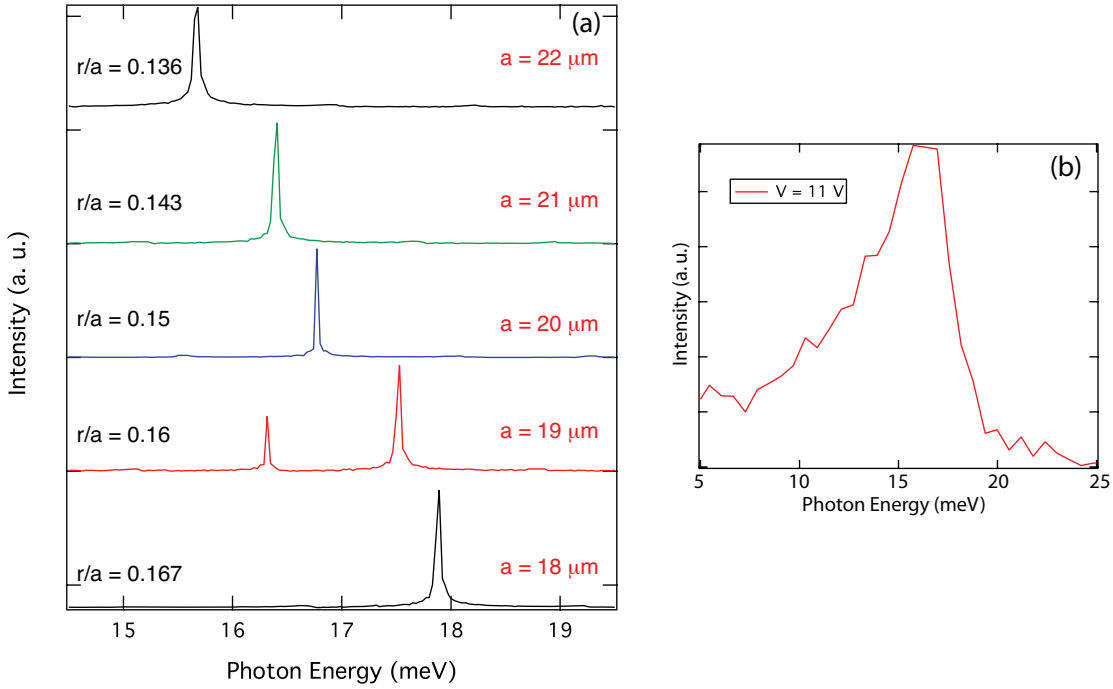

Fig. 4. (a) Optical spectra recorded from a series of five different devices with different PhC parameters at about the same applied bias (13.8 V). Most of the lasers show a single mode behavior and a progressive red shift tuning is observed by increasing the PhC lattice period. (b) Reference sub-threshold electro-luminescence spectrum obtained from a THz QCL based on the same active region and processed in a standard ridge waveguide configuration. The quality of the spectrum is limited by thermal noise due to the high doping levels (and high injected currents) of the active region. The measurements were performed at 7 K.

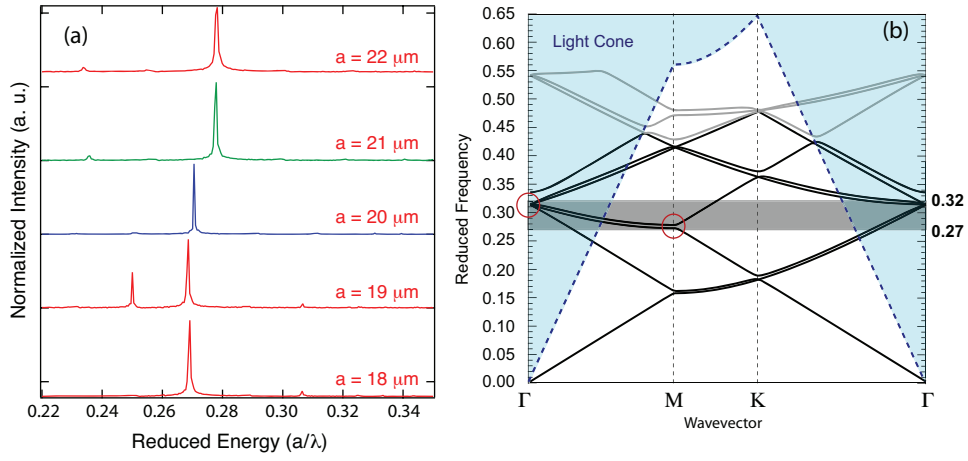

Fig. 5. (a) Optical spectra, as shown in Fig.4, plotted in reduced energy units. (b) Photonic band dispersion calculated for r = 3μm, and a = 22μm.

#91091 - $15.00 USD Received 21 Dec 2007; revised 29 Feb 2008; accepted 20 Mar 2008; published 1 Apr 2008

up to the LI rollover. For a ≥ 21, a second mode appears at reduced energy $a/\lambda = 0.305$ when the applied bias is high enough to allow a sufficient overlap of the gain curve with the high symmetry point Γ of the band dispersion. This aspect is clearly evidenced in Fig.6(a), where the spectral evolution, plotted in reduced units, as a function of the injected current is shown for a laser device with a = 22 μmand r = 3 μm. The transition from M-lasing to Γ-lasing occurs,

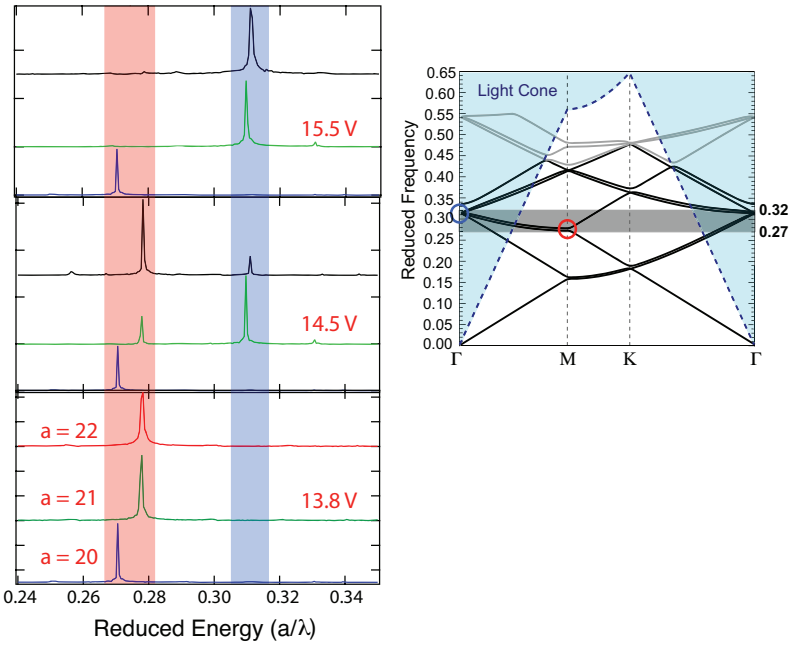

Fig. 6. (a) Spectral evolution, as a function of the applied bias voltage, plotted in reduced energy units from three different devices with lattice parameters "a" being respectively 20, 21, and 22 μm. The measurements were performed at 7 K. (b) Photonic band dispersion as in Fig.2.

in this case, at V$\geq$ 14.5 V and it progressively moves the laser emission intensity towards the Γ energy upon increasing the applied voltage. At V $>$ 15 V the transition is completed and the laser emission recovers to a single mode behavior at the Γ energy. The appearance of the Γ-mode at both high bias voltages and large PhC lattice constants is due to the high reduced energy of this high symmetry point that allow a sufficient overlap with gain curve only for a$\geq$21μm once the bias-induced Stark blueshift is large enough. Moreover, the Γ-modes present higher optical losses, if compared to the M or K-modes below the light cone, due to the k_z conservation, that couples them efficiently to the vacuum (a second order Bragg condition is automatically satisfied at the Γ point). Concerning this point, a significant slope increase in the integrated laser emission behavior is observed as a function of the injected current and therefore of the applied bias as shown in Fig.7 for a device with a = 21 μm and r = 3 μm. From this graph a nonlinear increase of the optical emission is observed as soon as the mode transition from the M-lasing to the Γ-lasing takes place, with a maximum intensity reached when the laser emission is single mode at the Γ energy.

4. Far-field emission

The far-field pattern of the laser devices is a key element necessary for the understanding of the lasing mechanism and light extraction. In this work the far-field pattern was scanned by a

#91091 - $15.00 USD Received 21 Dec 2007; revised 29 Feb 2008; accepted 20 Mar 2008; published 1 Apr 2008

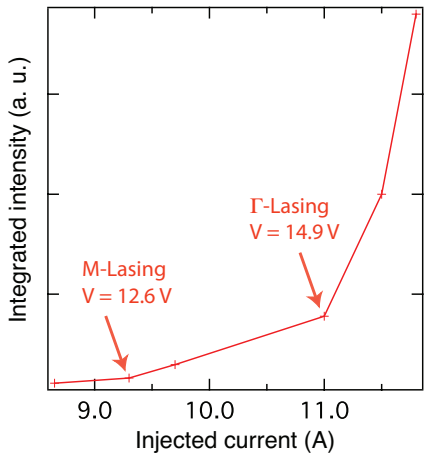

Fig. 7. Integrated spectral emission vs injected current plot at 7 K. A nonlinear increase of the lasing emission is observed when the spectrum shifts from a "M-emission" to a "Γ"-emission.

pyroelectric detector mounted on a double rotational stage that allows an angular scan close to 180° on θ and ϕ angles while the sample was mounted on a He-flow cryostat and kept at cryogenic temperature.

A typical unpolarized far-field pattern of our devices with a = 21 and r = 3, is shown in Fig.8(a) and (b) recorded at respectively at J = 725 A/cm^2 (V = 13.1 V) and, J = 890 A/cm^2 (V = 15.6 V). For the relative optical spectra that have been detected at similar bias the reader can refer to Fig.6 where is clearly shown that the mode jump previously discussed takes place between these two biases. A two-lobes symmetry is recovered for both injection currents, and although a variation in the intensity distribution over the sample surface is observed upon increasing of the injected current, no clear evidence of transverse mode transition in correspondence of the spectral change is noticed.

Although from numerical simulations, based on finite difference time domain (FDTD) algorithm, a two-lobes symmetry turns out to be a mode existing in a finite photonic lattice with triangular symmetry, we do believe that this pattern is strongly related to both the finite size of the device together with the rectangular shape of the contact pad. Indeed, the two lobes axis is always oriented parallel to the short side of the pad. One possible mechanism is that the edge of the metallic pad provides a feedback on the propagating surface plasmon excited by the laser mode, and that the mode shape reflects the surface plasmon mode pattern. At this point, it is worth noting that an even symmetry mode has been observed in similar devices at ≈ 8 μm wavelength in the presence of a rectangular contact pad [15]. In other words, the *true* transverse mode profile proper of the PhC structure is wiped out by the surface plasmon absorption re-emission mechanism in the metal layer.

In order to investigate the impact of a perturbation of the planar geometry of the devices on the light extraction mechanism and mode pattern, few samples have been fabricated by dry etching the PhC holes through the entire active region. Some preliminary results on one of these structures are shown in Fig.9 where both LIV curve and optical spectra are presented.

Also in this case the longitudinal mode evolution sees an abrupt transition from the M-modes to the Γ-mode upon increase of the applied voltage. Nevertheless, this device shows a significant increase of the output peak power (up to 20 mW), if compared to the previous devices, together with a very low threshold current density J_{th}= 375 A/cm^2. Moreover, two abrupt changes in

#91091 - $15.00 USD Received 21 Dec 2007; revised 29 Feb 2008; accepted 20 Mar 2008; published 1 Apr 2008

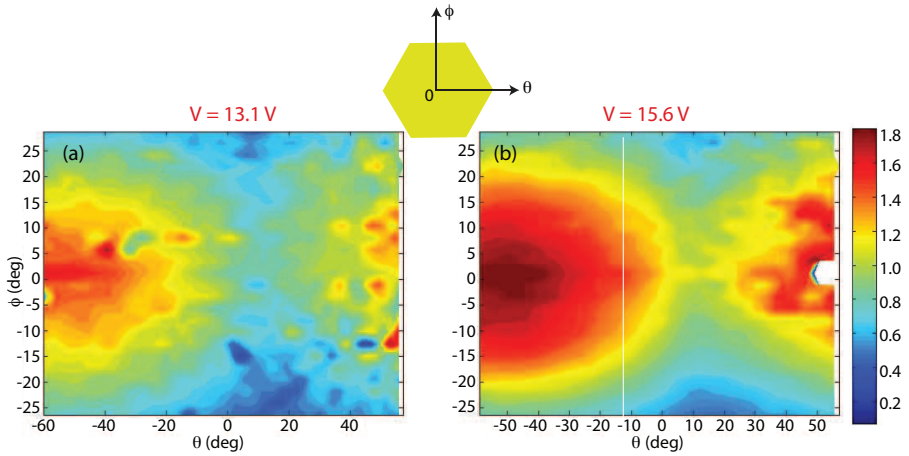

Fig. 8. Far-field emission patterns recorded from a device with a = 21μm and r = 3 μm at (a) V = 13.1 V and (b) V = 15.6 V corresponding to lasing emission attributed respectively to the M-point and the Γ-point of the PhC resonator. The (0;0) position corresponds approximately to the center of the hexagonal lattice of the laser sample. The measurements were performed at 20 K.

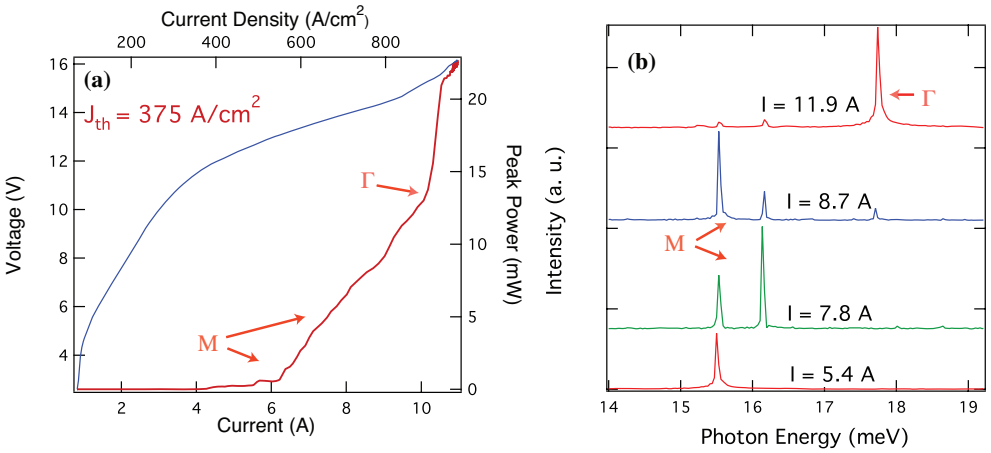

Fig. 9. (a) LIV curves of a deeply etched PhC laser with r/a = 0.136 (a = 22 μm and r = 3 μm). (b) Corresponding optical spectra evolution recorded at different bias voltages at 7 K.

#91091 - $15.00 USD Received 21 Dec 2007; revised 29 Feb 2008; accepted 20 Mar 2008; published 1 Apr 2008

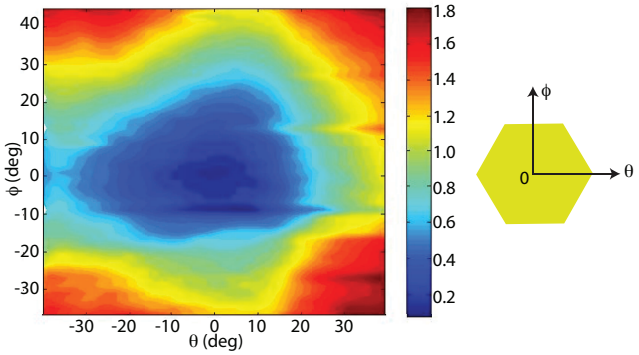

Fig. 10. Far-field emission pattern from the deeply etched PhC laser described above at a bias voltage V = 15 V (Γ-lasing). Also here the (0;0) position corresponds approximately to the center of the hexagonal lattice of the laser sample. The measurements were performed at 20 K.

slope efficiency are observed. The first one around 6 A of injected current corresponds spectrally to a single-mode to multi-mode transition on the M-symmetry point, whereas the second one occurs at I = 10 A where a transition from an M-mode to a Γ-mode lasing is spectrally observed (see Fig.9). We believe that this behavior is induced by an interplay between an increased quality factor of the optical cavity together with an improved light extraction efficiency associated to this structure geometry where the almost perfect planarity of the shallow-etched devices is perturbed.

This interpretation is supported by the far-field pattern recorded at 15 V bias voltage, correspondent to a Γ-lasing operation, shown in Fig.10. Here the optical mode appears in a four-fold geometry and with a different light intensity distribution, with respect to the un-etched samples, that suggests an enhanced optical feedback induced by the deep holes of the structure. However, also in this case the contact pad symmetry seems to play an important role in the mode distribution, and the overall external efficiency of the laser is still dominated by a surface plasmon mediated extraction mechanism.

5. Conclusions

In summary, we have demonstrated spectral control of surface laser emission in a 2D PhC-based THz QCL. A detailed analysis of the laser spectra shows that it is possible to attribute the emission lines to different transitions associated to high symmetry points of the PhC structure

#91091 - $15.00 USD Received 21 Dec 2007; revised 29 Feb 2008; accepted 20 Mar 2008; published 1 Apr 2008

and is therefore possible to control the spectral properties of the QCL by means of the PhC design.

The low output power shows also that it is extremely difficult to extract light vertically in connected planar PhC plasmonic structures due to the dominance of the plasmonic absorption in this direction in the double-metal waveguides. This interpretation is corroborated by the early results shown on deeply etched PhC QCLs.

Better results are expected on unconnected PhC cavities (pillar-based PhC) or by better exploiting the plasmon-mediated emission in the vertical direction.

#91091 - $15.00 USD Received 21 Dec 2007; revised 29 Feb 2008; accepted 20 Mar 2008; published 1 Apr 2008